# A nanometric window on fullerene formation in the interstellar medium: Insights from molecular dynamics studies

Cite as: J. Chem. Phys. 156, 154704 (2022); https://doi.org/10.1063/5.0069166 Submitted: 29 August 2021 • Accepted: 28 March 2022 • Accepted Manuscript Online: 29 March 2022 • Published Online: 19 April 2022





🧓 Abhishek Kumar Thakur, 匝 Krishna Muralidharan, Thomas J. Zega, et al.







# ARTICLES YOU MAY BE INTERESTED IN

A consistent and accurate ab initio parametrization of density functional dispersion correction (DFT-D) for the 94 elements H-Pu

The Journal of Chemical Physics 132, 154104 (2010); https://doi.org/10.1063/1.3382344

A deep potential model with long-range electrostatic interactions

The Journal of Chemical Physics 156, 124107 (2022); https://doi.org/10.1063/5.0083669

Two-exciton bound state quantum self-trapping in an extended star graph

The Journal of Chemical Physics 156, 155101 (2022); https://doi.org/10.1063/5.0087200

# Lock-in Amplifiers up to 600 MHz









# A nanometric window on fullerene formation in the interstellar medium: Insights from molecular dynamics studies

Cite as: J. Chem. Phys. 156, 154704 (2022); doi: 10.1063/5.0069166 Submitted: 29 August 2021 • Accepted: 28 March 2022 •







Published Online: 19 April 2022



Abhishek Kumar Thakur, 1 D Krishna Muralidharan, 1,2,3 D Thomas J. Zega, 1,2 and L. M. Ziurys 3,4,5,3

### **AFFILIATIONS**

- Department of Materials Science and Engineering, University of Arizona, Tucson, Arizona 85721, USA
- <sup>2</sup>Lunar and Planetary Laboratory, University of Arizona, 1629 E. University Blvd., Tucson, Arizona 85721, USA
- Department of Chemistry and Biochemistry, University of Arizona, Tucson, Arizona 85721, USA
- Department of Astronomy, Steward Observatory, University of Arizona, 933 North Cherry Ave., Tucson, Arizona 85721, USA
- <sup>5</sup>Arizona Radio Observatory, Steward Observatory, University of Arizona, 933 North Cherry Ave., Tucson, Arizona 85721, USA

# **ABSTRACT**

Understanding the fundamental mechanisms that underlie the synthesis of fullerene molecules in the interstellar medium (ISM) and in the environments of astrophysical objects is an open question. In this regard, using classical molecular dynamics, we demonstrate the possibility of in situ formation of fullerene molecules, such as C60 from graphite, which is known to occur in the ISM, in particular, circumstellar environments. Specifically, when graphite is subjected to thermal and mechanical stimuli that are typical of circumstellar shells, we find that the graphite sheet edges undergo significant restructuring and curling, leading to edge-induced interlayer-interactions and formation of mechanically strained five-membered-ring structural units. These units serve as precursors for the formation of fullerene structures, such as pristine and metastable C<sub>60</sub> molecules. The pathways leading to molecular C<sub>60</sub> formation consist of a series of steps that involve bondbreakage and subsequent local rearrangement of atoms, with the activation energy barriers of the rate-limiting step(s) being comparable to the energetics of Stone-Wales rearrangement reactions. The identified chemical pathways provide fundamental insights into the mechanisms that underlie  $C_{60}$  formation. Moreover, they clearly demonstrate that top-down synthesis of  $C_{60}$  from graphitic sources is a viable synthesis route at conditions pertaining to circumstellar matter.

Published under an exclusive license by AIP Publishing. https://doi.org/10.1063/5.0069166

# I. INTRODUCTION

The discovery that laser vaporization of graphite could lead to the formation of  $C_{60}$  buckminsterfullerene as well as other fullerene molecules ultimately led to the Nobel Prize for Curl, Kroto, and Smalley.1 These findings served as an important launchpad for the field of carbon nanotechnology.<sup>2</sup> They also provided the basis for interpreting spectroscopic signatures of astrochemical carbon species. However, deciphering the mechanisms that underlie the synthesis of fullerenes in the interstellar medium (ISM) and in the environments of astrophysical objects is an open question. Thus far, there is currently a lack of consensus on the formation of fullerenes in such environments. Progress on this front can

provide valuable insights into how large, pure-carbon compounds, such as fullerenes, are created in these environments where elemental carbon coexists with hydrogen, oxygen, nitrogen, and even sulfur. Recent experimental studies by Bernal et al.<sup>3</sup> suggested that fullerene cages can indeed be synthesized from presolar SiC grains out of graphitic layers formed through shock heating. Such a pathway provides a convenient solid-state driven reaction that eliminates competing gas-phase reactions involving other elements. Here, we expand on those findings and focus on utilizing atomistic computational techniques to examine the possibility of forming fullerene structures, in particular C<sub>60</sub> within solid-state bulk graphitic structures, at conditions pertaining to interstellar environments without explicitly resorting to reactions in the gas-phase.

a) Authors to whom correspondence should be addressed: krishna@email.arizona.edu and Iziurys@arizona.edu

### II. BACKGROUND

Broadly speaking, graphite as well as polycyclic aromatic hydrocarbons and hydrogenated amorphous carbon can all serve as precursor materials for fullerene formation. For synthesis from graphitic sources, multiple chemical pathways were proposed as viable routes for obtaining fullerene structures as discussed in Refs. 4 and 5. A majority of the proposed routes can be classified as "bottom-up." Specifically, in the bottom-up route, when hot carbon vapor is formed from graphite (via thermal, electric, electron-beam, or optical excitations), fullerene structures have been shown to coalesce from smaller clusters of gas-phase/vaporized carbon atoms. The bottom-up scenarios include (i) "shrinking hot giant route," where both upsizing and downsizing of fullerenes occur due to the spontaneous self-assembly and restructuring of carbon fragments and chains at high temperatures that lead to preferential formation of  $C_{60}$ ,  $C_{70}$  structures; <sup>5,6</sup> (ii) "the pentagon road," where curved structures turn into closed spheres by addition of carbon atoms that satisfy the isolated pentagon ring rule;7 (iii) "fullerene road," where C<sub>2</sub> fragments are regularly inserted leading to fullerene formation;<sup>8</sup> and (iv) "ring coalescence," where smaller ring-fragments unite to form larger fullerene molecules. In contrast to the bottom-up routes, Chuvilin et al.4 showed that graphene sheets could undergo restructuring at their edges, followed by sheet curling, resulting in fullerene (C60) molecules, indicating that top-down routes for fullerene formation are also possible.

In the context of establishing mechanisms for the synthesis of fullerenes in the ISM, the role of other elements, such as hydrogen, that are present along with carbon poses additional challenges. Recently, observations showed that both  $C_{60}$  and  $C_{70}$  are present in planetary nebulae and other circumstellar environments (see, e.g., Refs. 10 and 11), as well as in diffuse clouds (see, e.g., Ref. 12). It was also suggested that  $C_{60}^+$  occurs in diffuse gas (e.g., Ref. 13). Despite the increased identifications, a facile mechanism that can readily cohere sp<sup>2</sup>-hybridized carbon atoms together to form thermodynamically stable nanofragments and nanostructures in environments that are rich in hydrogen and other elements under typical astrophysical conditions has yet to be proposed (Ref. 14). In these astrophysical settings, bottom-up formation processes are thought to be unlikely, as timescales are too long to build to a 60-70 atom molecule, given typical interstellar densities and temperatures (e.g., Ref. 15). Top-down synthesis seems to be more viable, with either hydrogenated amorphous carbon ("HACs") or polycyclic aromatic hydrocarbons (PAHs) as the starting materials. Experimental work shows that fullerene-like structures can be generated in HACs (e.g., Refs. 16 and 17). Furthermore, studies by Tielens and collaborators (e.g., Refs. 18 and 19) and Berne et al.20 suggest that PAHs may be a route to  $C_{60}$  by a series of processes involving dehydrogenation, folding, and shrinking. However, in both cases, there are difficulties with intermediate steps, such as eliminating hydrogens in an H-rich gas.

Recently, Bernal *et al.*<sup>3</sup> conducted laboratory experiments where SiC grains were subjected to shock heating. As a result of the thermal treatment, a graphitic matrix was formed on the SiC surface, within which fullerene cages were detected. We note that the shock heating was to simulate conditions that SiC grains would be subjected to in interstellar and circumstellar envelopes, where they are known to form.<sup>20</sup> These findings are significant because they demonstrate the following: (i) fullerenes could be produced

within graphite in a top-down approach (i.e., in the solid-state and no requirement for gas-phase condensation and coalescence of fragments from carbon vapor), and (ii) there are alternative routes for production of fullerenes in astrophysical settings from presolar materials like SiC or *possibly graphite grains* that are commonly produced in carbon-rich circumstellar envelopes.<sup>21</sup>

The new insights provided by Bernal et al. clearly show that there are solid-state synthetic routes for fullerene formation. Furthermore, their study raises fresh questions on the fundamental mechanisms that govern the top-down formation of fullerene from pure graphitic sources. To this end, in this work, using classical molecular dynamics (MD), we have characterized the atomic dynamics in graphite grains that drives the formation of fullerene structures (especially  $C_{60}$ ) within graphite. We note that previously, MD was successfully implemented to examine high-temperature synthesis pathways of fullerene and fullerene-like caged structures from amorphous carbon<sup>22</sup> and gas-fragment clusters<sup>23</sup> as well as from nano-diamond clusters under high temperature conditions.<sup>24</sup> Building on these investigations, using MD simulations, we provide an atomistic window on the experimental observations of Bernal et al. and shed further light on the possibility of  $C_{60}$  synthesis from pure graphite grains under interstellar/circumstellar conditions. In addition, we elucidate possible reaction pathways and their respective kinetic barriers that underlie the formation of  $C_{60}$  in the ISM.

To simulate conditions pertaining to the ISM, we pay particular attention to the role of thermal and mechanical shock and examine their impact on the formation of fullerene structures within graphite. Carbon containing grains, such as SiC and graphite, created in the circumstellar envelopes of stars (e.g., Ref. 21 and references therein), can experience shock processing as the star leaves the asymptotic giant branch (AGB) of stellar evolution. Specifically, in the later part of the AGB, thermal pulses, created by a helium-shell flash, generate shock waves in the extended stellar atmosphere, which propagate into the envelope (e.g., Ref. 25). Dust grains entrained in the outflowing stellar wind can experience further shock waves at even higher velocities (>100 km/s) as the star transitions to a planetary nebula, which can raise the temperature of the material instantaneously to 1000 K and above. <sup>26–28</sup> Such shock can also include the impact and implantation of ions onto grain surfaces. <sup>29</sup>

Details on the simulation procedure are provided in Sec. III, while salient results on the chemical pathways for  $C_{60}$  are provided and discussed in Sec. IV.

# III. MOLECULAR DYNAMICS SIMULATION PROCEDURE

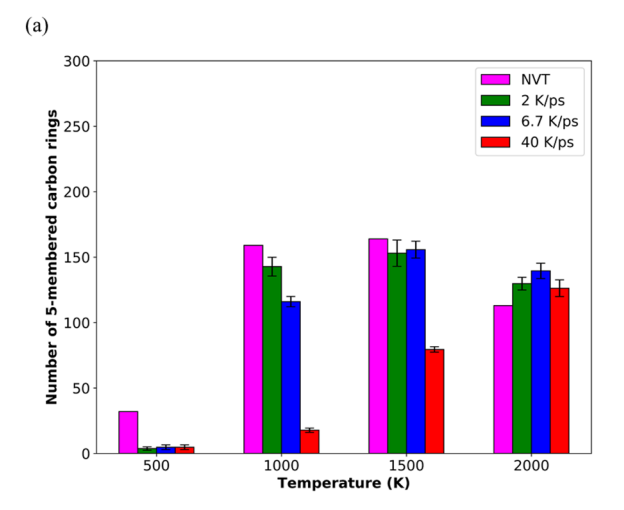
Classical molecular dynamics (MD) was used as the modeling tool to simulate the atomic-scale dynamics of graphite and examine the reaction pathways that could lead to the formation of "in situ" fullerene structures within graphite. To ensure computational accuracy, the LCBOP-II interatomic potential was used for describing the atomic interactions between carbon atoms. <sup>30</sup> We note that the LCBOP-II potential was implemented previously to examine the graphite to diamond transitions under astrophysical shock loading conditions, <sup>31,32</sup> as well as fullerenization of isolated nanodiamond grains. <sup>24</sup> Furthermore, the LCBOP-II potential is able to predict the energetics and structural characteristics of spherical and tubular fullerene molecules accurately.

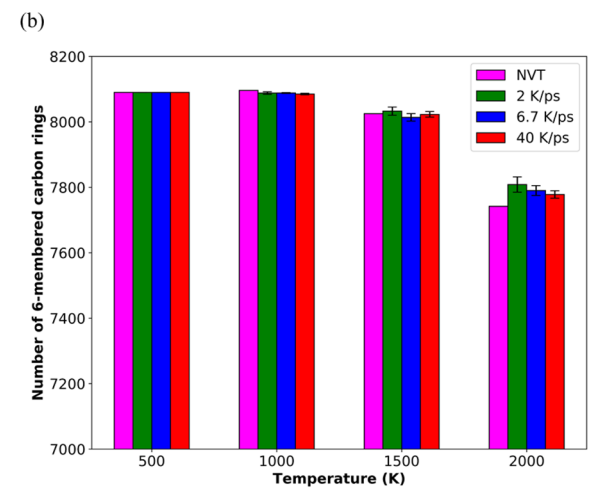
We used Large-scale Atomic/Molecular Massively Parallel Simulator (LAMMPS)<sup>33</sup> as the MD simulation engine in this work, and all simulations were carried out on the University of Arizona's high performance computing system. The simulated graphite system consists of 18 000 carbon atoms stacked in 10 layers contained initially within a 3D periodic cell. The lattice vectors  $(\vec{a}, \vec{b}, \vec{c})$  of the periodic cell equaled (in Å)

$$\begin{pmatrix} \vec{a} \\ \vec{b} \\ \vec{c} \end{pmatrix} = \begin{pmatrix} 73.68 & 0.00 & 0.00 \\ -36.84 & 63.8 & 0.00 \\ 0.00 & 0.00 & 33.48 \end{pmatrix}$$

An initial energy minimization step was carried out, followed by a constant number of atoms (N)–constant pressure (P)–constant temperature (T) (NPT) run using the Nose–Hoover barostat for 100 ps at 100 K to ensure that the system was essentially at zero pressure (in bars) in order to match the near-vacuum, low-temperature conditions in the ISM. This was followed by an NVE run for 100 ps to ensure that the system was well equilibrated without any drift in the total energy. Here, NVE refers to the microcanonical ensemble, where the number of atoms (N) and the simulation-cell volume (V) are kept fixed, and since neither the temperature nor pressure of the system is fixed, the total energy of system (E) is conserved. An MD time step of 1 femtosecond was used unless otherwise noted.

To emulate conditions corresponding to the ISM, specifically in pulsating circumstellar shells, the equilibrated graphite system was subjected to rapid heating and mechanical shock. During the "thermal shock" simulations, the bottom two layers were kept fixed, while periodic boundary conditions were removed in all three directions by introducing a vacuum-spacing of 5 nm in all three directions. The removal of periodic boundaries creates free-edges (predominantly armchair or zigzag with a few dangling-bond atoms) and free-surfaces, typical of experimental conditions, while fixing the bottom two layers is akin to simulating a thicker substrate. Prior to the shock simulations, the system was equilibrated at 100 K under NVT conditions [i.e., constant volume (V) and temperature (T)] for 50 ps using the Nose-Hoover thermostat, after which the temperature of the system was ramped from 100 K to 2000 K under three different thermal ramp-rates: 40, 6.7, and 2 K/ps. Once 2000 K was reached, each of the systems was allowed to run for at least 50 ps under NVE conditions to examine if the system was stable after the release of the thermal shock. 2000 K corresponds to typical temperatures experienced by dust grains under shock heating in astrophysical conditions, and hence, we examined the response up to 2000 K. Furthermore, based on past MD investigations of shock compression of graphite under comparable conditions<sup>32</sup> (i.e., shock velocities in the range of a few Km/s), temperature spikes similar to the thermal shock rates studied in this work were observed, providing a sound basis for the choices used in our studies. However, to ensure appropriate comparisons and to bound properly the effects of the large thermal ramp rates on the structural evolution of the system under study, we also examined NVT-equilibrated structures at four different temperatures (500, 1000, 1500, and 2000 K), with the equilibration time equaling 500 ps. The NVT-equilibrated structures provide the baseline for evaluating and understanding the effect of thermal shock-rates on graphite. Furthermore, the NVT





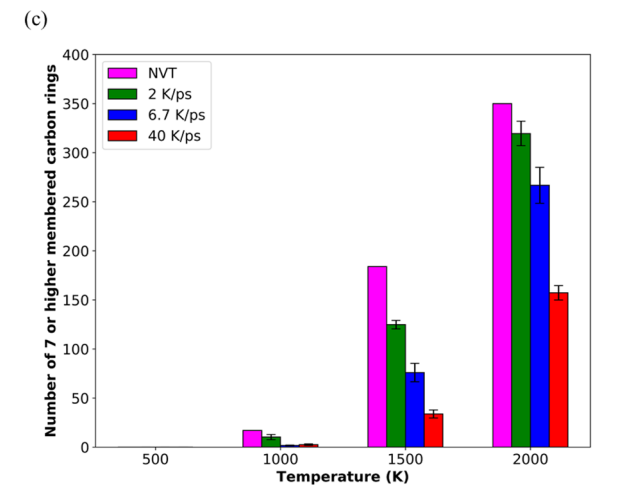


**FIG. 1.** Number-evolution of (a) five-membered (5R), (b) six-membered (6R), and (c) seven or higher membered carbon rings (LR) as a function of temperature for different rates of thermal shock (2, 6.7, and 40 K/ps). For comparison, we have also provided the corresponding NVT simulation data.

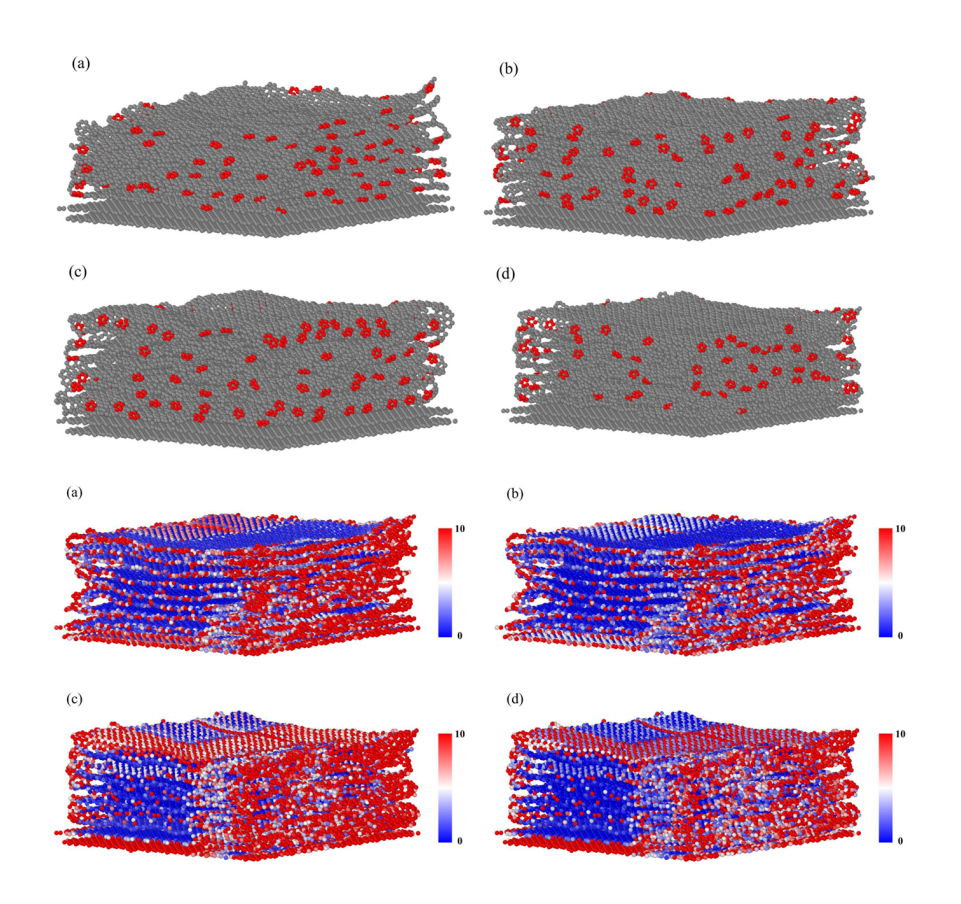


FIG. 2. Snapshots of thermally shocked graphite matrix at 2000 K, when thermal shock equals (a) 40 K/ps, (b) 7 K/ps, and (c) 2 K/ps. For comparison, (d) we have also provided the snapshot of the NVT system at 2000 K. The five-membered carbon rings are shown in red; a similar spatial distribution for the LR rings is also seen, but for brevity, we only provide the 5R spatial distribution.

FIG. 3. Snapshots of the graphite matrix under NVT conditions: (a) shear strain map at 1000 K; (b) volumetric strain map at 1000 K; (c) shear strain map at 2000 K; and (d) volumetric strain map at 2000 K.

simulations represent conditions where the grains can experience high temperatures in the circumstellar environments for much longer times as compared to single shocks. We note that multiple shocks can lead to sustaining high temperatures for much longer durations as compared to single shocks. For all of the above thermal shock simulations, four distinct sets of MD-runs were carried out in order to provide averages and statistical bounds to our findings.

In addition to thermal heating, we also examined the effect of mechanical shock on graphite. Similar to the thermal heating setup, equilibration of vacuum-encompassed graphite at 100 K was followed by subjecting it to a positive pressure of 1 GPa for 100 ps, after which the system was simulated under NVE conditions for 50 ps. For the system under study, the pressure and energy were well-equilibrated before the end of the shock-simulation, as was also verified by the lack of energy drift during the NVE stage. In astrophysical settings, dust grains can be subject to shock velocities of a

fraction of and to  $\sim 100$  km/s, which correspond to non-equilibrium, transient internal pressures greater than equal to 1 GPa. In this context, our work provides a baseline for understanding the role of shock compression on the structural evolution of graphite as well.

The RINGS software package<sup>34</sup> was used for characterizing the structural evolution of graphite when subjected to thermal and mechanical shocks. The RINGS code allows for analyzing graphite in terms of the constituent ring-structure; while pristine graphite contains only six member (6R) rings, fullerene molecules contain both five-member (5R) and 6R rings. Thus, knowing the ring structure can help in identifying regions within graphite that show fullerene-like structural features.

In order to complement MD simulations, we also carried out the nudged elastic band (NEB) transition state search algorithm<sup>35</sup> to locate transition paths and activation barriers underlying formation

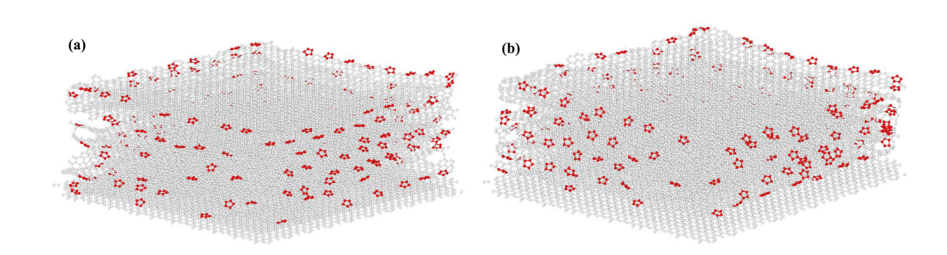


**FIG. 4.** Snapshots of the simulated graphite matrix under NVT conditions at (a) 1000 K and (b) 1500 K. The five-membered carbon rings are shown in red.

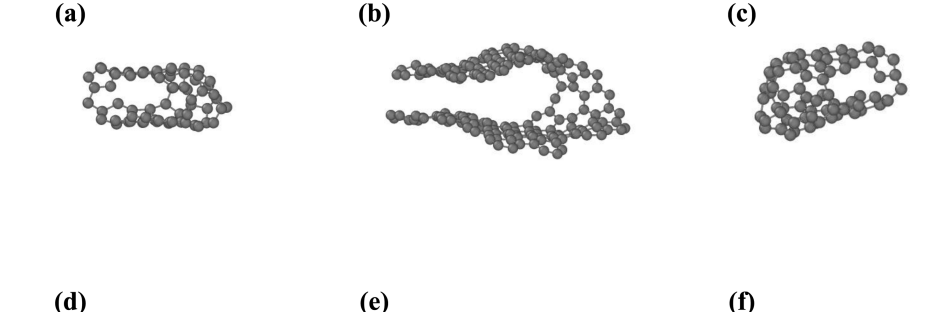


**FIG. 5.** Examples of identified carbon fragments that can serve as precursors for formation of fullerene structures: (a)  $C_{70}$ , (b)  $C_{180}$ , (c)  $C_{72}$ , (d)  $C_{38}$ , (e)  $C_{120}$ , and (f)  $C_{60}$ .

of fullerene structures located within the "shocked" graphitic systems. For these purposes, we used the multiple replica-based NEB module<sup>35</sup> as implemented within LAMMPS.

### IV. RESULTS AND DISCUSSION

As a first step, we present MD results pertaining to the evolution of the simulated graphitic structures when subject to shock heating. While graphite sheets solely consist of connected six-membered carbon rings (6R), fullerenes consist of both fivemembered carbon rings (5R) and 6R units, where the 5R units are associated with the strain that arises due to curvature of the fullerene structures. Thus, we pay particular attention to the formation and evolution of 5R units in conjunction with evolving strain as the graphite is subjected to thermal shock. In this regard, a striking aspect of all simulations is the interplay among the thermal shock rate, instantaneous temperature, and the corresponding rapid increase in the population of the 5R units. We note that prior to shock heating, when the periodic system (sans free-edges and surfaces) was equilibrated at 100 K, there was no formation of 5R units, and noticeable formation of 5R units was observed only for the system with free-edges was shocked or equilibrated to 500 K and above.

Figure 1(a) provides a comparison of the respective 5R populations as a function of instantaneous temperature for the shocked

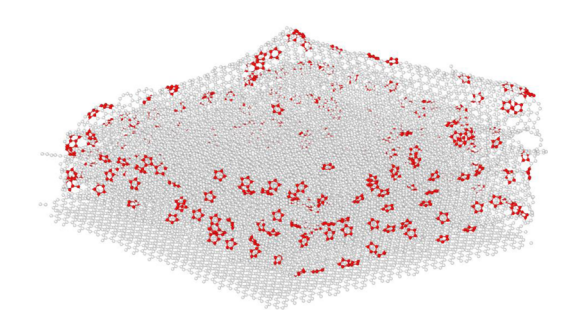


**FIG. 6.** Snapshot of the simulated graphite matrix when subjected to a pressure of 1 GPa. The five-membered carbon rings are shown in red.

systems as well as for the system that was equilibrated under NVT conditions for the corresponding temperatures. We note that we carried out the ring-analysis on the snapshot obtained at the end of equilibration for the NVT systems. As seen in Fig. 1(a), except for the extremely fast thermal shock case (40 K/ps), which shows a monotonic increase in the number of 5R units, the maximum number of 5R units is seen at 1500 K for the other systems. The 6R population shows a slight uptick at 1000 K for the NVT case and then decreases past 1500 K [Fig. 1(b)], with the uptick associated with some inter-sheet coupling at the sheet edges; furthermore, similar to the 5R evolution, we see a distinct increase in the number of larger-ring (LR) units (i.e., rings that have greater than or equal to seven carbon atoms) between 1000 and 2000 K as shown in Fig. 1(c). Based on Figs. 1(a)-1(c), one can infer that the formation of the 5R and LR rings are thermally driven, and beyond 1500 K, 5R units are relatively less stable as compared to LR units, indicating the preference for larger, more open ring structures at high temperatures. In addition, by comparing the evolution of the ring structures of the shocked systems with the corresponding NVT system (which represents the baseline equilibrated structure for a given temperature), one can also conclude that the respective timescales of the shock simulations determine the corresponding ring-populations. That is, the longer the residence time at or close to a given temperature, the higher the probability of forming thermally driven 5R and LR

To further interpret the evolution of the 5R and LR unit populations, we present structural snapshots of the respective systems at



**FIG. 7.** 60 membered sheet of carbon atoms, which served as the starting structure for the formation of a spherical  $C_{60}$  molecule.

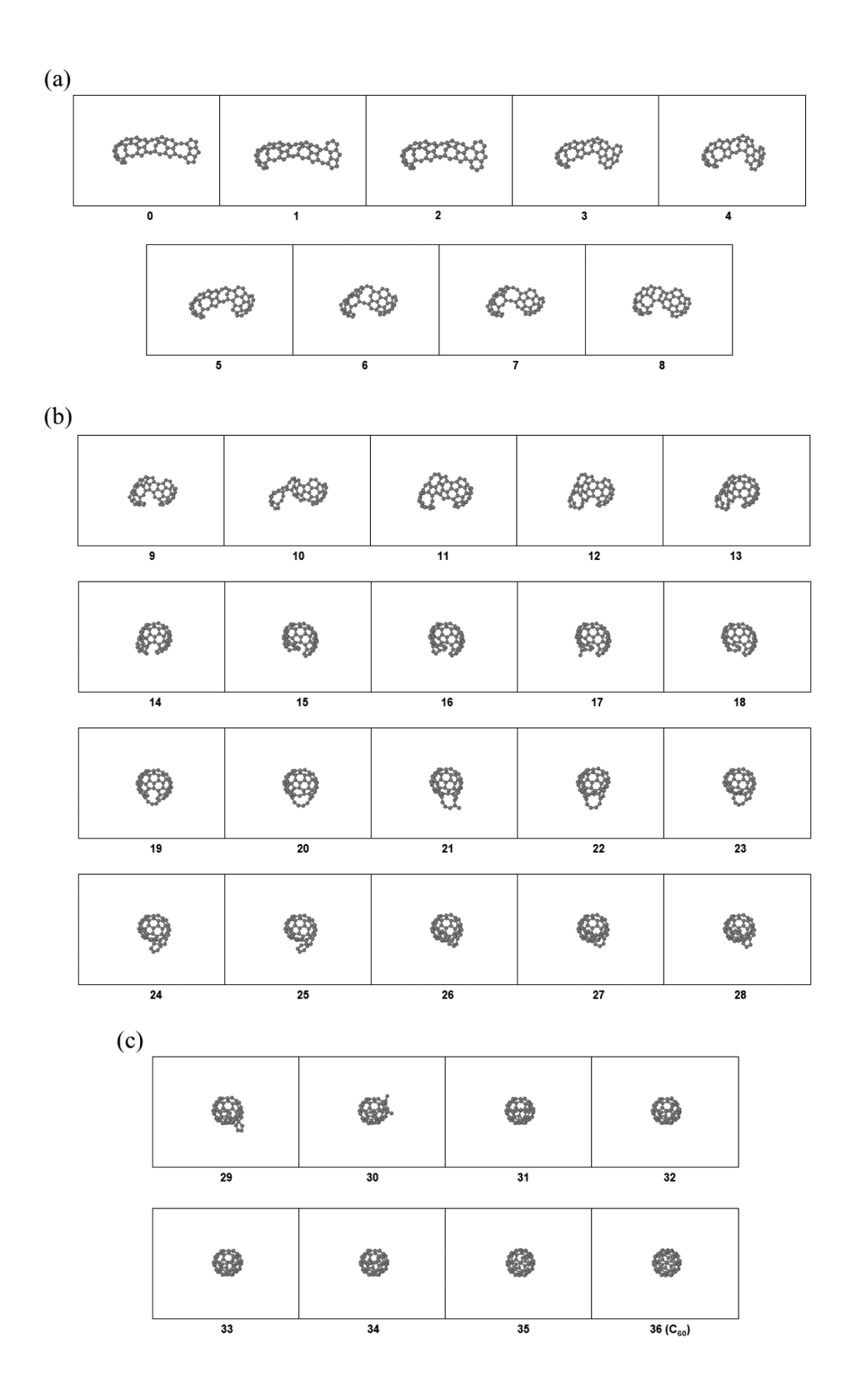


**FIG. 8.** Different stages underlying the formation of the spherical  $C_{60}$  molecule from the open carbon sheet. Snapshots depicting the evolution of the carbon fragment in (a) stage 1, (b) stage 2, and (c) stage 3. Note that the numbering of the snapshots corresponds to the identified steps involved in the transformation.

2000 K as shown in Figs. 2(a)-2(d). Superimposed on these snapshots are the spatial distribution of the 5R units. The 5R units are predominantly found at the graphite sheet edges, and furthermore, as seen in Figs. 2(a)-2(d), there is strong coupling of graphite sheets at the edges. For clarity, while we only show the spatial distribution of the 5R units, the LR spatial distribution is also similar to that of 5R. Importantly, the 7R and larger units are found in close proximity to the 5R units at the sheet edges. Interestingly, the inter-sheet coupling results in the formation of many close semi-spherical and tubular structures that are studded with 5R (and 6R) units, reminiscent of fullerene-like structures.

In order to understand the reasons behind the predominance of 5R (and LR) units at the sheet edges, we examine the spatial variation of volumetric and shear atomic-strain as a function of temperature. For brevity and clarity, we focus only on the NVT results, but the findings are applicable to the shock heating systems as well. Figures 3(a)-3(d) show the respective volumetric and shear strain maps at 1000 and 2000 K, respectively, and it is clear that the strains experienced by the edge-atoms is much higher than the "bulk" atoms and increases with temperature.

To complement the strain maps, we also present structural snapshots of the equilibrated system at 1000 and 1500 K [Figs. 4(a) and 4(b)], while the corresponding 2000 K snapshot is already given in Fig. 2(d). As seen from Figs. 3 and 4, with increasing strain at the edges, the edge-atoms, which are undercoordinated as compared to atoms within the bulk of the graphite sheets, undergo much larger displacements, enabling bonding between edge-atoms belonging to neighboring sheets. As a result of the inter-sheet coupling, we see curling of the edges and formation of closed semi-spherical and tubular structures at the edges of the graphite structure. The coupling of sheets when accompanied by increased strain within the graphitic structure leads to structural rearrangement, especially at these coupled regions, as seen by the formation of 5R, additional 6R, as well as LR units. While there is a direct spatial correlation between the formation of 5R, LR and additional 6R rings and the increased strain at the sheet edges, a more dedicated study is required to elucidate the fundamental mechanisms that relate the interplay between strain and the mechanistic pathways that lead to the respective ringformations at the sheet edges. Such an examination will be part of a follow-up study.

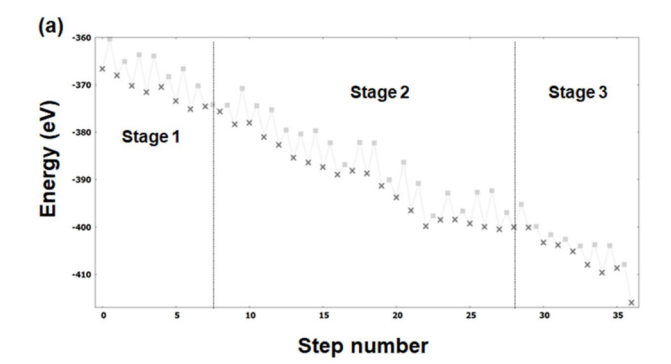
Nevertheless, our observations are also consistent with the work of Posligua *et al.*,<sup>36</sup> where it was shown that graphite sheet edges were susceptible to strain-driven inter-layer coupling, promoting the formation of carbon nanostructures consisting of concentric loops in few-layer graphitic structures. In addition, Koskinen *et al.* also demonstrated that reconstruction at graphene-edges can lead to formation of adjacent heptagon (7R) and 5R units or isolated 5R units <sup>37</sup>

As mentioned earlier, the presence of 5R units, especially in regions where tubular and semi-spherical domains are found, is of particular importance, given that fullerene molecules, such as  $C_{60}$  and  $C_{70}$ , have both 6R and 5R rings. Thus, based on these observations, we can clearly suggest that rapid thermal heating of graphite can also lead to the formation of curved domains that possess the appropriate structural units that can serve as precursors to fullerene molecules. In this context, we present some of the "precursor" fragments that were formed within the shocked graphite in Figs. 5(a)-5(f). We note that each of the fragments have

characteristics that can serve as precursors to the formation of closed pristine fullerene structures.

Similar to the thermal heating simulations, when graphite was subjected to rapid compression, extensive coupling of neighboring sheets accompanied by the formation of 5R and LR units was observed, as shown in Fig. 6. This result suggests that, irrespective of the stimulus (thermal or mechanical shock), graphite undergoes significant transformation, leading to formation of "sub-structures" characteristic of fullerene molecules.

Given the rather short timescales associated with MD simulations, directly obtaining pristine spherical  $C_{60}$  fullerenes within the shocked graphitic structure was not possible. However, having demonstrated the ability to form fullerene-like cages within graphite, we now examine the possibility of synthesizing pristine  $C_{60}$  molecules from sub-structures found within thermally or mechanically shocked graphite. We consider domains within the shocked graphitic structures and examine structural transformations coupled with transition state search algorithms that would lead to the formation of pristine  $C_{60}$  molecules, with the acknowledgment that much longer residence times at high temperatures are required to enable such transformations.



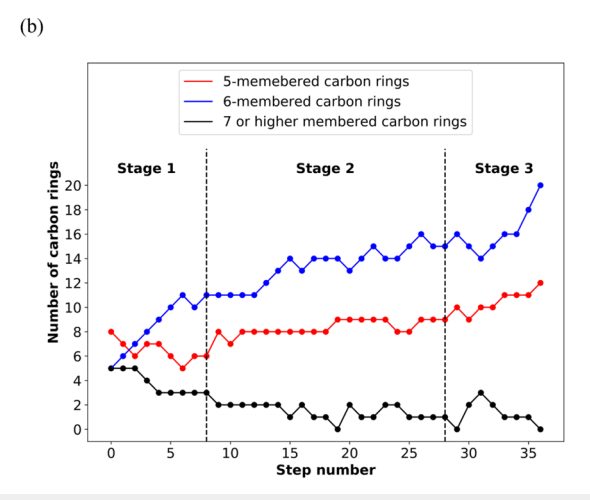


**FIG. 9.** (a) Step-by-step evolution of potential energy (x) and the corresponding transition states (black colored rectangle) associated with the transformation from the open carbon sheet to the spherical  $C_{60}$  molecule; (b) corresponding evolution in the population of the carbon rings.

As an illustrative example, we present the chemical pathways that underlie the transformation to a  $C_{60}$  molecule from a fragment identified within the graphitic structure (Fig. 7) and quantify both the energetics as well as the kinetic barriers that characterize this transformation. We intentionally chose a 60-atom fragment found at the sheet edges that is sheet-like, contains 5R units, but does not possess any intrinsic curvature. The implicit assumption is that requiring a flat sheet to form a spherical  $C_{60}$  fullerene structure within the graphite matrix may require additional restructuring steps, thereby representing an "upper limit" in terms of

underlying energetics and activation barriers that characterize the ensuing chemical pathway.

To characterize the transformation, we examine the structural rearrangements that underlie the chemical pathways that convert the identified fragment to a pristine  $C_{60}$  molecule in isolation (i.e., in the gas-phase) as well as within the graphitic matrix (i.e., in the solid state). The NEB method is used to identify activation barriers and rate-limiting steps in the transformation and a minimum of 32 replicas (i.e., interpolated intermediate structures between each step) were used for identifying the transformation pathway between

**TABLE I.** Critical Steps underlying the transformation of the identified carbon sheet into  $C_{60}$ .

Transition step	Stage	Activation barrier (gas phase) (eV)	Activation barrier (solid state) (eV)	Salient features of transformation process
Initial carbon sheet to structure 1	1	6.27	4.77	Conversion of a 5R unit to a 6R unit at sheet edge to ensure isolation of 5R units. $9R + 5R\rightarrow 8R + 6R$
Structure 3 to 4	1	7.64	6.75	Combination of 7R and 5R to form adjacent 6R rings. $7R + 5R \rightarrow 6R + 6R$
Structure 5 to 6	1	6.83	6.64	Restructuring a LR (9R) to form a 6R unit. $5R + 9R \rightarrow 6R + 11R$
Structure 9 to 10	2	7.58	6.70	Restructuring a LR (8R) to form adjacent 5R and 6R units. $8R \rightarrow 6R + 5R$
Structure 14 to 15	2	6.74	3.97	Combination of LR units to form a 6R unit and another LR units.7R + 8R $\rightarrow$ 6R + 10R
Structure 18 to 19	2	6.46	5.61	Restructuring of an LR (9R) to a 5R unit. $9R \rightarrow 5R$
Structure 20 to 21	2	7.43	5.29	Transformation of an LR (7R) to a 6R unit. $7R \rightarrow 6R$
Structure 25 to 26	2	7.03	5.80	Rearrangement of "tail" atoms to form adjacent $5R$ and $6R$ units. $7R \rightarrow 8R + 6R$
Structure 26 to 27	2	7.62	6.65	Rearrangement of LR to form an additional 5R unit. $8R \rightarrow 5R + 8R$

each step. For simplicity, we identified the restructuring steps for the gas-phase transformation and transposed every step within the graphite matrix. We, therefore, did not pursue other routes with perhaps lower activation barriers.

Figures 8(a)-8(c) shows a step-by-step illustration of the identified chemical pathway that underlies the transformation. A total of 36 elementary steps were identified, with each step involving combinations of atomic displacements or bond-breakage. Broadly, the transformation can be divided into three stages: stage 1 consists of curling the flat sheet accompanied by an increase in 6R, especially at the ends of the sheet; stage 2 consists of further restructuring leading to eliminating LR units and forming isolated 5R units in addition to 6R units ultimately closing the sheet into a spherical structure; stage 3 consists of successive rearrangements within the spherical structure leading to the formation of a pristine  $C_{60}$  molecule.

The potential energy (i.e., the binding energy) of every energy-minimized intermediate structure corresponding to each step as well as the respective activation energy barriers between steps is provided in Fig. 9(a). We note that we only provide the potential energy of the gas-phase cluster in Fig. 9(a); furthermore, the observed trend in potential energy variation is very similar for both the gas-phase and solid-state transformations, respectively.

As evident from Fig. 9(a), we see a near-monotonic decrease in potential energy as we progress from the flat sheet to the pristine  $C_{60}$  molecule. The potential energy variation suggests that the transformation is energetically favorable and should be viable purely from a thermodynamic point of view. For further analysis, we also provide the corresponding step-by-step evolution in the ring structure in Fig. 9(b), which sheds light on the correlation between increased stabilization of the structure due to an increase in the number of 6-C and 5-C rings as the structure folds from a sheet into a curved closed-structure.

From a kinetics viewpoint, there are multiple activation barriers that represent critical rate-limiting steps that characterize the transformation into  $C_{60}$  [shown in Fig. 9(a)]. Table I provides the respective activation barriers of these critical rate-limiting steps associated with the transformation. For each of these critical steps, we have provided the underlying structural rearrangement mechanisms, which are defined in terms of interconversion between different ring structures. For all of these identified steps, a common feature is the creation of at least one lower-member unit from LR units. The corresponding "fragment" geometries for the identified steps are given in Fig. 10, where the "participating" atoms are duly identified, while select solid-state geometries corresponding to the transformation process are given in Fig. 11. As noted in Table I, the activation barriers for the solid-state rate-limiting steps are always lower than that of the corresponding gas-phase cases. Furthermore, the maximum activation barrier we obtained for the solid-state case was ~6.75 eV; the underlying ring-conversion mechanism for this rate-limiting step involved the combination of a 5R and a 7R unit to form a pair of 6R units, mediated by a carbon-carbon bond rotation, which interestingly relates partly to the inverse Stone-Wales rearrangement mechanism. Furthermore, the observed activation barriers of all critical transformation steps are lower than other comparable high-temperature (~2000 K) restructuring mechanisms, such as the Stones-Wales (SW) rearrangement or the edge-rearrangement and curling of graphene sheets that lead to formation of  $C_{60}$ .

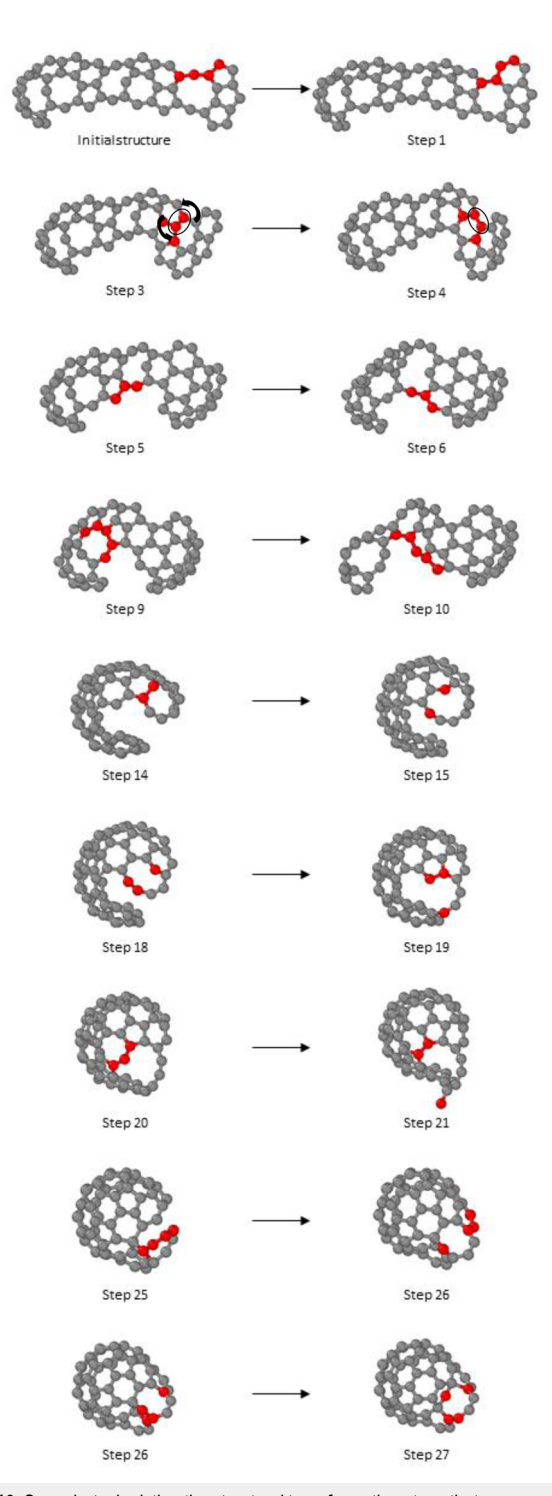


**FIG. 10.** Snapshots depicting the structural transformation steps that correspond to the steps identified in in Table I. For convenience, we have colored specific atoms in red; these atoms participate in the structural transformation corresponding to each of the identified steps. Of particular interest is the structural transformation between steps 3 and 4, which corresponds to the rate-limiting step; here, there is rotation of a carbon–carbon bond leading to conversion of a 7R + 5R unit to a pair of 6R units

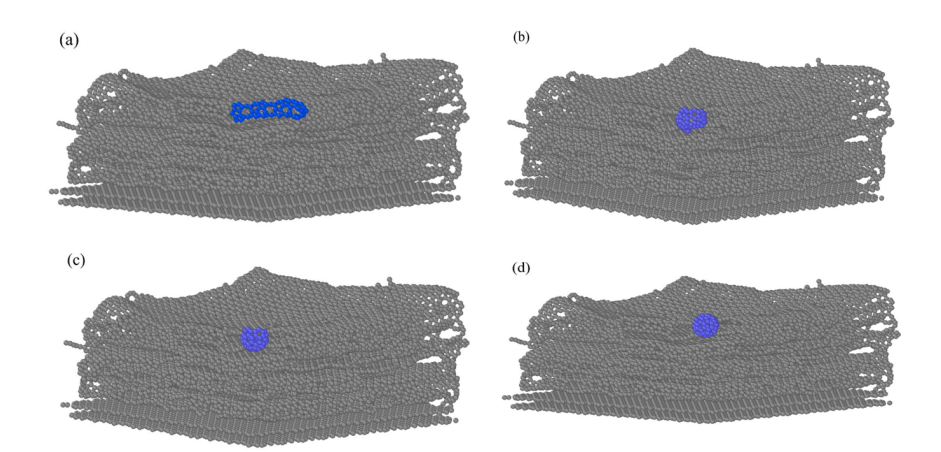


**FIG. 11.** Select snapshots of the transforming carbon fragment (in blue) within the graphite matrix. The snapshots correspond to (a): the initial carbon sheet, (b) step 15, (c) step 27, and (d) spherical  $C_{60}$ .

The maximum activation barrier we obtained for the solid-state case was  ${\sim}6.75$  eV, which is less than barriers associated with other comparable high-temperature ( ${\sim}2000$  K) restructuring mechanisms, such as Stones–Wales rearrangement or the edge-rearrangement and curling of graphene sheets that lead to formation of  $C_{60}$ .

For more detailed comparisons, we first examine the energetics of Stone–Wales (SW) defects that arise in carbon nanostructures, such as graphene and fullerene, due to the underlying high temperature processing conditions. The structural rearrangement that underlies the formation of SW defects involves a topological restructuring of carbon bonds, leading to a 90° rotation of a carbon bond and a conversion of a group of 4 6R rings into two pairs of 7R and 5R rings, respectively. The SW transformation has been shown to be an important if not the primary rearrangement mechanism that drives the growth mechanisms of fullerene molecules from smaller clusters<sup>38</sup> and coalescence of fullerene cages. <sup>39,40</sup>

For the SW defect, the estimated activation barrier in fullerene tubes and graphene range between 6.5 and 9.2 eV,  $^{41-43}$  while Fthenakis and Lathiotakis showed that the barrier reduces to 5 eV under high strain.  $^{44}$  We note that using the LCBOP potential, we obtained the formation energy of SW in graphene to be 5 eV and the activation barrier to be 8.9 eV, both of which compare well with a DFT-based analysis.  $^{43}$  Importantly, the estimated activation barrier of the rate-limiting steps associated with the  $C_{60}$  transformation examined in this work is lower than the estimated SW activation barrier and, thus, strengthens the central thrust of this work. Furthermore, the identified pathways do not explicitly include SW rearrangements, which points to the fact that there has to be other equivalent transformation pathways to form  $C_{60}$  fullerene molecules from precursors, and thus, this work only represents one such mechanism.

The NEB search performed in this work only focused on examining the transformation of a single carbon fragment into a  $C_{60}$  buckyball. The rather irregular topology of the chosen fragment as compared to more ordered structures of graphene and smaller fullerene fragments could be a possible reason for obtaining "non-SW" based transformation pathways underlying the formation of  $C_{60}$  as shown in Table I. In this regard, a more exhaustive analysis of various fragments needs to be carried out to identify if indeed

non-SW based transformation pathways can also underlie the formation of  $C_{60}$  fullerene molecules from other precursors, thereby providing a more nuanced as well as a comprehensive understanding of formation of  $C_{60}$  in astrophysical settings.

To provide further context for this work, we note that in a prior investigation by Chuvilin *et al.*,  $^4$  the formation of  $C_{60}$  from single sheet graphene was demonstrated. The thermodynamic barrier for  $C_{60}$  formation was shown to be around 12 eV, which is much higher than the estimated kinetic barriers in our work. Importantly, their work also demonstrated the need for the presence of 5R at the graphene sheet edge, and their estimated barrier was based on the creation of the 5R units at the sheet-edge. In this work, we demonstrate that high-temperature and high-strain conditions provide the needed impetus to form these 5R units, and these conditions can be realized under astrophysical settings, such as the ISM. Furthermore, the distinguishing feature of our work is the consideration of the role of the multi-layered graphite sheet edges, which was much more favorable for  $C_{60}$  synthesis as compared to a single sheet in the work of Chuvilin *et al.*.

Also relevant is the use of classical MD simulations to model the high temperature formation (3000 K) of fullerene-like caged structures from a random distribution of isolated atoms in gasphase<sup>23</sup> or from carbon nanotubes,<sup>45</sup> as well as the formation of  $C_{60}$  from amorphous carbon clusters.<sup>22</sup> In the latter work,<sup>22</sup> Sinistsa *et al.* demonstrated that at high temperatures (~2500 K), the carbon cluster can undergo atomic restructuring, leading to the formation of many closed carbon structures, including spherical  $C_{60}$ . In another closely related work, Sinitsa *et al.* examined high temperature ( $\geq$ 2400 K) migration of sp hybridized carbon atoms to quench defects in fullerenes containing odd number of carbon atoms, leading to formation of stable fullerene isomers.<sup>46</sup>

Following the work of Sinitsa,<sup>22</sup> we subjected the sheet-like fragment to high temperatures ( $\sim$ 2000 K), which led to the formation of a closed metastable elliptical  $C_{60}$  structure [Fig. 12(a)]. The unique aspect of the obtained elliptical  $C_{60}$  structure was the fact that it contained the same number of 5R (12) and 6R (20) units. The energy of the metastable  $C_{60}$  structure was  $\sim$ 0.1 eV/atom higher than the pristine  $C_{60}$  molecule.

Other MD simulations that enable suitable comparisons with our work include studies of nanodiamond and graphite

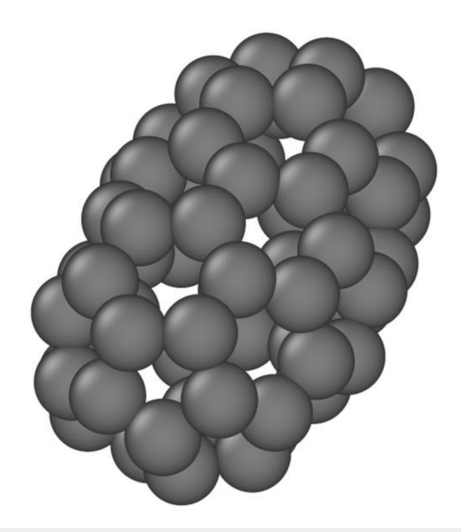


**FIG. 12.** Snapshot of the metastable  $C_{60}$  structure possessing the same number of five-membered and six-membered rings as the spherical  $C_{60}$  molecule.

under extreme mechanical and thermal perturbations. <sup>23</sup> Specifically, Los *et al.* <sup>24</sup> demonstrated that upon heating to 3000 K, an isolated spherical 3 nm sized nanodiamond grain could undergo fullerenization, initiated from the diamond surface, resulting in the formation of "carbon onions (CO)" studded with 5R and larger rings in addition to unconverted 6R rings. The CO shells were correlated with large radii fullerene-like molecules, though none of them were structurally identical to pristine spherical fullerene molecules, such as  $C_{60}$ . Furthermore, a key difference in Los *et al.*, <sup>24</sup> as compared to our study, is the fact that the spherical nature of the nanodiamond is particularly suited for the formation of the fullerenized CO shells. In our work, it is the coupling of the graphite sheets and the subsequent strain-induced structural transformation that leads to the formation of fullerene and fullerene-like structures.

# V. CONCLUSIONS

Using classical MD simulations, we examine the structural response of graphite to elevated temperature and mechanicaldeformation conditions which can arise due to single or multiple thermal and mechanical shock events relevant to circumstellar and interstellar conditions. Under both thermal and mechanical stimuli, the graphite sheet edges undergo significant strain accompanied by layer-curling and inter-layer bonding at the edges. Interestingly, these observations were very weakly dependent on the timescales of the thermal stimulus (via shock) pointing to the fact that layer-curling and inter-layer bonding should occur even over the rapid timescales associated with a single thermal shock event. The edge-coupling is characterized by the formation of strained five-membered carbon rings, which along with the presence of six-membered rings, adorn hemispherical and tubular structures. Such structures serve as precursors for the formation of pristine  $C_{60}$  molecules. In particular, using transition-state search methods, we examine and quantify the chemical transformation that enables the formation of  $C_{60}$  from precursor structures within the graphite matrix. The estimated activation barriers for rate-limiting steps that

underlie the transformation are less than the kinetic barrier for formation of Stone–Wales defects, indicating the ability to form  $C_{60}$  molecules from and within graphite grains in the ISM. We note that the identified transformation pathway represents one among possibly other routes for top-down synthesis of  $C_{60}$ . Importantly, the identified chemical pathways provide fundamental insights into the solid-state mechanisms that underlie  $C_{60}$  formation, indicating that that top-down synthesis of  $C_{60}$  from graphitic sources should be the primary synthesis route at conditions pertaining to the ISM. Furthermore, the results and insights obtained in this work provide independent confirmation of the findings of Bernal  $et\ al.$ , where rapid heating of graphite was shown to produce spherical carbon structures reminiscent of fullerenes.

# **ACKNOWLEDGMENTS**

The authors thank Dr. Jacob Bernal for useful discussions. This work was supported by NSF Grant No. AST-1907910.

### **AUTHOR DECLARATIONS**

### **Conflict of Interest**

The authors have no conflicts to disclose

# **DATA AVAILABILITY**

The data that support the findings of this study are available from the corresponding author upon reasonable request.

# **REFERENCES**

- <sup>1</sup>H. W. Kroto, J. R. Heath, S. C. O'Brien, R. F. Curl, and R. E. Smalley "C<sub>60</sub>: Buckminsterfullerene," Nature **318**, 162 (1985).
- <sup>2</sup>Carbon Nanomaterials, edited by Y. Gogotsi and V. Presser (Taylor & Francis, 2013).
- $^{3}$  J. J. Bernal, P. Haenecour, J. Howe, T. J. Zega, S. Amari, and L. M. Ziurys, "Formation of interstellar  $C_{60}$  from silicon carbide circumstellar grains," Astrophys. J. **883**, L43 (2019).
- <sup>4</sup>A. Chuvilin, U. Kaiser, E. Bichoutskaia, N. A. Besley, and A. N. Khlobystov, "Direct transformation of graphene to fullerene," Nat. Chem. **2**, 450 (2010).
- $^5$ S. Irle, G. Zheng, Z. Wang, and K. Morokuma, "The  $C_{60}$  formation puzzle solved: QM/MD simulations reveal the shrinking hot giant road of the dynamic fullerene self-assembly mechanism," J. Phys. Chem. B 110, 14531–14545 (2006).
- <sup>6</sup>J. Y. Huang, F. Ding, K. Jiao, and B. I. Yakobson, "Real time microscopy, kinetics, and mechanism of giant fullerene evaporation," Phys. Rev. Lett. 99, 175503 (2007).
  <sup>7</sup>H. W. Kroto and K. McKay, "The formation of quasi-icosahedral spiral shell carbon particles," Nature 331, 328–331 (1988).
- <sup>8</sup>J. R. Heath, "Synthesis of C<sub>60</sub> from small carbon clusters: A model based on experiment and theory," in *Fullerenes: Synthesis, Properties and Chemistry of Large Carbon Clusters*, ACS Symposium Series, edited by G. S. Hammond and V. J. Kuck (American Chemical Society, 1991), Vol. 481, pp. 1–23.
- <sup>9</sup>J. M. Hunter, J. F. Fye, E. J. Roskamp, and M. F. Jarrold, "Annealing carbon cluster ions—a mechanism for fullerene synthesis," J. Phys. Chem. **98**, 1810–1818 (1992)
- $^{10}$ J. Cami, J. Bernard-Salas, E. Peeters, and S. E. Malek, "Detection of  $C_{60}$  and  $C_{70}$  in a Young planetary nebula," Science **329**(5996), 1180–1182 (2010).
- $^{11}$ Y. Zhang and S. Kwok, "On the detections of  $C_{60}$  and derivatives in circumstellar environments," Earth, Planets Space 65, 1069 (2013).
- $^{12}$ O. Berné and A. G. G. M. Tielens, "Formation of buckminsterfullerene ( $C_{60}$ ) in interstellar space," Proc. Natl. Acad. Sci. **109**, 401–406 (2012).
- $^{13}$ S. Spieler, M. Kuhn, J. Postler, M. Simpson, R. Wester, P. Scheier, W. Ubachs, X. Bacalla, J. Bouwman, and H. Linnartz, " $C_{60}^{+}$  and the diffuse interstellar bands: An independent laboratory check," Astrophys. J. **846**, 168 (2017).

- <sup>14</sup>S. Kwok and Y. Zhang, "Mixed aromatic-aliphatic organic nanoparticles as carriers of unidentified infrared emission features," Nature 479, 80–83 (2011).
- <sup>15</sup>O. Berné, J. Montillaud, and C. Joblin, "Top-down formation of fullerenes in the interstellar medium," Astron. Astrophys. 577, A133 (2015).
- <sup>16</sup>W. W. Duley and A. Hu, "Fullerenes and proto-fullerenes in interstellar carbon dust," Astrophys. J. Lett. **745**, 2008 (2012).
- $^{17}$ Y. Carpentier, G. Féraud, E. Dartois, R. Brunetto, E. Charon, A. T. Cao, L. D'Hendecourt, P. Bréchignac, J. N. Rouzaud, and T. Pino, "Nanostructuration of carbonaceous dust as seen through the positions of the 6.2 and 7.7 μm AIBs," Astron. Astrophys. 548, A40 (2012).
- <sup>18</sup>J. Zhen, P. Castellanos, D. M. Paardekooper, H. Linnartz, and A. G. G. M. Tielens, "Laboratory formation of fullerenes from PAHS: Top down interstellar chemistry," Astrophys. J. Lett. 797(2), L30 (2014).
- <sup>19</sup>W. Zhang, Y. Si, J. Zhen, T. Chen, H. Linnartz, and A. G. G. M. Tielens, "Laboratory photochemistry of covalently bonded fluorene clusters: Observation of an interesting PAH bowl-forming mechanism," Astrophys. J. 872, 38 (2019).
- <sup>20</sup>L. M. Ziurys, "The chemistry in circumstellar envelopes of evolved stars: Following the origins of the elements to the origins of life," Proc. Natl. Acad. Sci. 103, 12274–12279 (2006).
- <sup>21</sup> T. J. Bernatowicz, T. K. Croat, and T. L. Daulton, "Origin and evolution of carbonaceous presolar grains in stellar environments," in Meteorites and the Solar System II, edited by D. S. Lauretta and H. Y. McSween, Jr. (The University of Arizona Press, Tucson, AZ, 2006), pp. 109–126.
- <sup>22</sup> A. S. Sinitsa, I. V. Lebedeva, A. M. Popov, and A. A. Knizhnik, "Transformation of amorphous carbon clusters to fullerenes," J. Phys. Chem. C 121, 13396–13404 (2017).
- <sup>23</sup>Y. Yamaguchi and S. Maruyama, "A molecular dynamics simulation of the fullrene formation process," Chem. Phys. Lett. **286**, 336–342 (1998).
- <sup>24</sup>J. H. Los, N. Pineau, G. Chevrot, G. Vignoles, and J.-M. Leyssale, "Formation of multiwall fullerenes from nanodiamonds studied by atomistic simulations," Phys. Rev. B 80, 155420 (2009).
- <sup>25</sup>S. Höfner and H. Olofsson, "Mass loss of stars on the asymptotic giant branch," Astron. Astrophys. Rev. 26, 1 (2018).
- <sup>26</sup>G. García-Segura, R. E. Taam, and P. M. Ricker, "Common envelope shaping of planetary nebulae. III. The launching of jets in Proto-Planetary nebulae," Astrophys. J. 914, 111 (2021).
- <sup>27</sup>M. N. Sevenster and J. M. Chapman, "A shock-excited OH maser in a post-asymptotic giant branch envelope?," Astrophys. J. 546, L119 (2001).
- <sup>28</sup>G. C. Van de Steene and P. A. M. van Hoof, "Shock emission in the bipolar post-AGB star IRAS 16594-4656," Astron. Astrophys. 406, 773–781 (2003).
- <sup>29</sup>P. R. Heck, F. Gyngard, U. Ott, M. M. M. Meier, J. N. Ávila, S. Amari, E. K. Zinner, R. S. Lewis, H. Baur, and R. Wieler, "Interstellar residence times of presolar SiC dust grains from the Murchison carbonaceous meteorite," Astrophys. J. **698**, 1155–1164 (2009).

- <sup>30</sup> J. H. Los, L. M. Ghiringhelli, E. J. Meijer, and A. Fasolino, "Improved long-range reactive bond-order potential for carbon. I. Construction," Phys. Rev. B 72, 214102 (2005).
- <sup>31</sup> H. Xie, F. Yin, T. Yu, J. T. Wang, and C. Liang, "Mechanism for direct graphite-to-diamond phase transition," Sci. Rep. 4, 5930 (2014).
- <sup>32</sup>N. Pineau, L. Soulard, L. Colombet, T. Carrard, A. Pellé, P. Gillet, and J. Clérouin, "Molecular dynamics simulations of shock compressed heterogeneous materials. II. The graphite/diamond transition case for astrophysics applications," J. Appl. Phys. 117, 115902 (2015).
- <sup>33</sup>S. Plimpton, "Fast parallel algorithms for short-range molecular dynamics," J. Comput. Phys. 117, 1–19 (1995).
- <sup>34</sup>S. Le Roux and P. Jund, "Ring statistics analysis of topological networks: New approach and application to amorphous GeS<sub>2</sub> and SiO<sub>2</sub> systems," Comput. Mater. Sci. **49**, 70–83 (2010).
- <sup>35</sup>G. Henkelman, B. P. Uberuaga, and H. Jónsson, "A climbing image nudged elastic band method for finding saddle points and minimum energy paths," J. Chem. Phys. **113**, 9901 (2000).
- <sup>36</sup>V. Posligua, J. Bustamante, C. H. Zambrano, P. J. F. Harris, and R. Grau-Crespo, "The closed-edge structure of graphite and the effect of electrostatic charging," RSC Adv. 10, 7994 (2020).
- <sup>37</sup>P. Koskinen, S. Malola, and H. Häkkinen, "Self-passivating edge reconstruction of graphene," Phys. Rev. Lett. 101, 115502 (2008).
- <sup>38</sup>B. R. Eggen, M. I. Heggie, G. Jungnickel, C. D. Latham, R. Jones, and P. R. Briddon, "Autocatalysis during fulleren growth," Science 272(5258), 87–90 (1996).
- <sup>39</sup>Y. Zhao, R. E. Smalley, and B. I. Yakobson, "Coalescence of fullerene cages: Topology, energetics, and molecular dynamics simulations," Phys. Rev. B 66, 195409 (2002).
- <sup>40</sup>Y. Zhao, B. I. Yakobson, and R. E. Smalley, "Dynamic topology of fullerene coalescence," Phys. Rev. Lett. 88(18), 185501 (2002).
- <sup>41</sup> M. Kabir, S. Mukherjee, and T. Saha-Dasgupta, "Substantial reduction of Stone-Wales activation barrier in fullerene," Phys. Rev. B 84, 205404 (2011).
- <sup>42</sup>L. G. Zhou and S.-Q. Shi, "Formation energy of Stone–Wales defects in carbon nanotubes," Appl. Phys. Lett. **83**, 1222 (2003).
- <sup>43</sup> L. Li, S. Reich, and J. Robertson, "Defect energies of graphite: Density-functional calculations," Phys. Rev. B 72, 184109 (2005).
- <sup>44</sup>Z. G. Fthenakis and N. N. Lathiotakis, "Graphene allotropes under extreme uniaxial strain: An *ab initio* theoretical study," Phys. Chem. Chem. Phys. 17, 16418 (2015).
- <sup>45</sup>G. Zheng, S. Irle, M. Elstner, and K. Morokuma, "Quantum chemical molecular dynamics model study of fullerene formation from open-ended carbon nanotubes," J. Phys. Chem. A **108**(15), 3182–3194 (2004).
- <sup>46</sup> A. S. Sinitsa, I. V. Lebedeva, Y. G. Polynskaya, A. M. Popov, and A. A. Knizhnik, "Molecular dynamics study of sp-defect migration in odd fullerene: Possible role in synthesis of abundant isomers of fullerenes," J. Phys. Chem. C 124(21), 11652–11661 (2020).